Binary black hole merger gravitational waves and recoil in the large mass ratio limit

Pranesh A. Sundararajan,[1,*] Gaurav Khanna,[2] and Scott A. Hughes[1]

[1]*Department of Physics and MIT Kavli Institute, MIT, 77 Massachusetts Avenue, Cambridge, Massachusetts 02139, USA*

[2]*Department of Physics, University of Massachusetts, Dartmouth, Massachusetts 02747, USA*

(Received 1 March 2010; published 5 May 2010)

Spectacular breakthroughs in numerical relativity now make it possible to compute spacetime dynamics in almost complete generality, allowing us to model the coalescence and merger of binary black holes with essentially no approximations. The primary limitation of these calculations is now computational. In particular, it is difficult to model systems with large mass ratio and large spins, since one must accurately resolve the multiple length scales that play a role in such systems. Perturbation theory can play an important role in extending the reach of computational modeling for binary systems. In this paper, we present first results of a code that allows us to model the gravitational waves generated by the inspiral, merger, and ringdown of a binary system in which one member of the binary is much more massive than the other. This allows us to accurately calibrate binary dynamics in the large mass ratio regime. We focus in this analysis on the recoil imparted to the merged remnant by these waves. We closely examine the ''antikick,'' an antiphase cancellation of the recoil arising from the plunge and ringdown waves, described in detail by Schnittman *et al.* We find that, for orbits aligned with the black hole spin, the antikick grows as a function of spin. The total recoil is smallest for prograde coalescence into a rapidly rotating black hole, and largest for retrograde coalescence. Amusingly, this completely reverses the predicted trend for kick versus spin from analyses that only include inspiral information.

DOI: 10.1103/PhysRevD.81.104009 PACS numbers: 04.25.Nx, 04.30.−w, 04.30.Db

I. INTRODUCTION AND BACKGROUND

A. Modeling binary systems in general relativity

After roughly three decades of effort, numerical relativity can now model nearly arbitrary binary black hole configurations. Following Pretorius' pioneering ''breakthrough'' calculation [1], and then the successes of the Brownsville and Goddard groups using techniques that required only modest modifications to the methods they used before the breakthrough [2,3], the past few years have seen an explosion of activity. Recent work has studied the impact of the many physical parameters that describe binaries, such as mass ratio [4,5], spin and spin alignment [6–9], and eccentricity [10,11]. As numerical models have improved, analytic tools for modeling binary systems [12] and connecting numerics and analytics have likewise matured. In particular, the *effective one-body* (EOB) [13–16] approach to binary dynamics, which maps the dynamics of a binary to that of a point particle moving in an ''effective'' spacetime corresponding to a deformed black hole, has been found to outstandingly describe the outcome of numerical relativity calculations after some adjustable parameters in the EOB framework are calibrated to numerical calculations [17–20]. Our understanding of the two-body problem in general relativity has never been better.

These efforts are largely motivated by the need for accurate models of coalescing black holes to detect and measure merger signals in the data of gravitational-wave (GW) detectors. Black holes with masses of roughly 10^6–$10^9 M_\odot$ indisputably reside at the cores of essentially every galaxy with a central bulge [21,22]. In the hierarchical growth of structure, these black holes will form binaries as their host galaxies merge and grow [23]; estimates of how often such binaries form indicate that the proposed space-based detector LISA [24,25] should be able to measure at least several and perhaps several hundred coalescences over a multiyear mission lifetime [26]. There is already a catalog of candidate binaries in this mass range, such as active galaxies with double cores [27–29], systems with doubly peaked emission lines [30,31], and systems that appear to be periodic or semiperiodic, such as the blazar OJ287 [32]. The last year or so of the binary's life will generate GWs at frequencies to which LISA is sensitive; measuring those waves will make it possible to precisely map the distribution of cosmic black hole masses and spins, opening a new observational window onto the high-redshift growth of cosmic structure.

Less massive black hole binaries (several to several hundred $M_\odot$) will be targets for the ground-based GW detector network, currently including LIGO [33], Virgo [34], and GEO [35], and hopefully including the proposed detectors LCGT [36], AIGO [37], and the ''Einstein Telescope'' [38] in the future. Formation scenarios and event rate estimates in this band are much less certain, since the demographics of the relevant black holes and scenarios for them to form binaries are not as well understood as in the supermassive range. However, scenarios involving dynamic binary formation in dense clusters suggest that this network can plausibly expect an interesting event rate [39–43], strongly motivating the construction of binary merger models for these detectors.

*P. A. S. is currently a Desk Strategist at Morgan Stanley and Co. Inc., 1585 Broadway, New York, NY 10036, USA

Finally, moving back to the LISA band, binaries in which one member is much less massive than the other are expected to be an important source. Such extreme mass ratio binaries are created when a stellar mass secondary (~ 1–$100 M_\odot$) is scattered through multibody interactions onto a highly relativistic orbit of a roughly $10^6 M_\odot$ black hole in the center of a galaxy. Though rare on a galaxy-by-galaxy basis, enough galaxies will be in the range of LISA that the number measurable is expected to be several dozen to several hundreds [44]. The waves from these binaries largely probe the quiescent spacetimes of their larger (presumably Kerr) black hole, making possible precision tests of the strong-field nature of black hole spacetimes [45].

In short, astrophysical binary black holes will come in a wide range of mass ratios. Computational models must be able to handle systems with mass ratios ranging from near unity, to millions to one. Each mass m sets a length scale Gm/c^2 which the code must be able to resolve. Large mass ratios require codes that can handle a large dynamic range of physically important length scales.

Perturbation theory is an excellent tool for modeling binaries with very large mass ratios. In this limit, the binary's spacetime is nearly that of its largest member, with the smaller member acting to distort the metric from the (presumably) exact Kerr solution of that "background." It is expected that tools based on perturbation theory will be crucial for modeling extreme mass ratio systems described above (mass ratios of 10^4:1 or larger). Even for less extreme systems, perturbative approaches are likely to contribute important wisdom, working in concert with tools such as numerical relativity and the effective one-body approach.

The foundational examples of such an analysis are the papers of Nagar, Damour, and Tartaglia [46] and of Damour and Nagar [47]. In that work, the EOB framework is used to construct the quasicircular late inspiral and plunge of a small body into a nonrotating black hole. Regge-Wheeler-Zerilli methods [48,49] are then used to compute the GWs that arise from a small body that follows that trajectory into the larger black hole. Those authors use this large mass ratio system as a "clean laboratory" for investigating binary dynamics, and advocate using these techniques as a tool for probing delicate issues such as the form of the waves that arise from the plunge, and the matching of the final plunge waves to the late ringdown dynamics of the system's final black hole.

Our goal here is to develop a similar toolkit based on perturbation theory applied to spinning black holes. We have developed two perturbation theory codes which we use to model different aspects of binary coalescence. Both codes solve the Teukolsky equation [50], computing perturbations to the curvature of a Kerr black hole. One code works in the frequency domain [51,52], which works well for computing the averaged flux of quantities such as energy and angular momentum carried by GWs. The other code works in the time domain [53,54], which is excellent for calculating the aperiodic GW signature of an evolving source. As originally proposed in Ref. [55], we have developed a hybrid approach which uses the best features of both the time- and frequency-domain codes to model the full coalescence process. (Although our ultimate goal is to develop a set of tools similar to those developed by Damour, Nagar, and Tartaglia, we note that our techniques are the moment largely numerical, as opposed to the mixture of numerical and analytic techniques developed in Refs. [46,47]. It would be worthwhile to connect the work we present here to the body of EOB work, but have not yet begun doing so in earnest.)

As we were completing this paper, a perturbation-theory-based analysis of binary merger was presented by Lousto *et al.* [56]. Their analysis does not use the Teukolsky equation, but is otherwise very similar in style and results to what we do here. In particular, they note as we do here that the perturbation equations terminate the merger waveform in a set of ringdown waves in a very natural way, thanks to the manner in which the equation's source redshifts away as the infalling body approaches the large black hole's event horizon. This behavior was also pointed out and exploited by Mino and Brink [57] in their (largely analytic) perturbative analysis of recoil from waves from the late plunge. We expand on this point in more detail at appropriate points later in the paper.

As our use of the Teukolsky equation requires, we assume that a binary can be well described by a small body moving in the spacetime of a (much larger) Kerr black hole. We first build the worldline that the smaller body follows as it slowly inspirals and then plunges into the black hole. We assume that, early in the coalescence, the small body moves on a geodesic of the background Kerr spacetime. Using the frequency-domain perturbation theory code to compute their rates of change, we allow the energy E, angular momentum L_z, and Carter constant Q of this configuration to evolve. (In fact, we confine ourselves to equatorial orbits in this analysis, so $Q = 0$ throughout the binary's evolution.) This drives the smaller body in an adiabatic inspiral through a sequence of orbits, until we approach the last stable orbit of the large black hole.[1]

We then make a transition to a plunging orbit, using the prescription of Sundararajan [58] which in turn generalized earlier work by Ori and Thorne[2] [59]. By properly connecting the adiabatic inspiral to a plunge, we make a full worldline describing the small body's coalescence with the

[1]At present, we do not include the conservative impact of self forces. These forces *are* included in the EOB-framework analyses of Damour, Nagar, and Tartaglia.

[2]A similar approach to the transition from inspiral plunge, but valid for arbitrary mass ratios and presented using the EOB framework, was developed by Buonanno and Damour [14], and appeared in press before Ref. [59].This approach is used in Refs. [46,47] to compute the transition from the slow, adiabatic inspiral to plunge.

larger black hole. This worldline gives us the source for our time-domain perturbation theory code, from which we compute the GWs generated by the system as the small body evolves from the (initially near geodesic) inspiral through the plunge and merger. The waves which we compute in this way have qualitatively the same "inspiral, merger, ringdown" structure seen in numerical relativity simulations, though much work remains to quantify the degree of overlap.

As an illustration of the utility of our perturbative toolkit, we focus in this paper on the problem of GW recoil. Studies of GW recoil have been particularly active in recent years; we review this problem and its literature in the next subsection.

B. Gravitational-wave recoil

The asymmetric emission of GWs from a source carries linear momentum. The system then recoils to enforce global conservation of momentum. Early work demonstrated the principle of this phenomenon [60,61]; Bekenstein [62] appears to have been the first to appreciate the important role it could play in astrophysical problems. Much recent work has focused on the recoil imparted to the merged remnant of binary black hole coalescence.

The first estimates of binary black hole kick were made by Fitchett [63]. He treated the gravitational interaction as Newtonian and included the lowest order mass and current multipoles needed for GW emission to compute the recoil velocity. This early calculation predicted that recoil velocities could approach thousands of km/s, which is greater than the escape velocity for many galaxies. Because of his restriction to low-order radiation formulas, and his use of Newtonian gravity to describe binary dynamics, it was clearly imperative that Fitchett's calculations be revisited; a prescient analysis by Redmount and Rees [64] particularly argued for the need to account for the effect of black hole spins in the coalescence.

Over the past several years, quite a few calculations have substantially improved our ability to model the recoil in general relativity. The various approaches can be grouped as follows:

(i) *Black hole perturbation theory:* As discussed extensively above, black hole perturbation theory is a good tool for describing binaries involving a massive central black hole (of mass M) and a much less massive companion (of mass μ). Shortly after Fitchett's pioneering binary calculation, Fitchett and Detweiler examined whether strong-field gravity changed the conclusions using perturbation theory [65]. Twenty years later, Favata, Hughes, and Holz [66] argued that, properly extrapolated, reasonable results can be obtained for quantities such as the integrated black hole kick up to a mass ratio $\mu/M \sim \mathcal{O}(0.1)$. Unfortunately, the Favata *et al.* analysis has a rather large final error since the frequency-domain tools they use do not work well at modeling the GWs arising from the final plunge of the smaller body into the large black hole. One of our goals in this analysis is to revisit that calculation and reduce those substantial error bars.

Another application of perturbation theory is the "close-limit approximation," [67] which describes the last stages of a merging binary as the dynamics of a distorted single black hole. Sopuerta, Yunes, and Laguna [68] applied the close-limit approximation to describe the final waves from unequal mass binaries, obtaining results that compare very well with those that have since been computed within "full" numerical relativity.

Finally, Mino and Brink [57] used perturbative techniques to model the waves from the plunge, quantifying the manner in which the geometry of the final infall impacts the kick imparted to the binary. As already mentioned, their analysis also took advantage of the manner in which the source redshifts away as the infalling body approaches the larger black hole's event horizon.

(ii) *Post-Newtonian (PN) theory:* PN theory describes the spacetime and the motion of bodies in the spacetime as an expansion in the Newtonian gravitational potential Gm/rc^2 (where m is a characteristic system mass, and r a characteristic black hole separation). Blanchet, Qusailah, and Will [69] used an approach based on this expansion to substantially improve estimates of the recoil from the final plunge and merger; though consistent with the results from [66], they were able to reduce the error bars by a substantial factor. More recently, Le Tiec, Blanchet, and Will [70] combined a PN inspiral with a close-limit computation of the merger and ringdown to compute the recoil for the coalescence of nonspinning black holes. This analysis is quite similar in spirit to the one we present here, though it does not use perturbation theory throughout.

(iii) *Numerical relativity:* Not long after it first became possible to model the coalescence of two black holes in numerical relativity, this became the technique of choice for computing black hole recoil. No other technique is well suited to computing wave emission and spacetime dynamics for very asymmetric, strong-field configurations which are likely to produce strong GW recoils. Numerical relativity was needed to discover the so-called "superkick" configuration: an alignment of spin and orbital angular momentum which results in a kick of several thousand kilometers per second [71–73]. In most configurations, the kick tends to be substantially smaller, peaking at a few hundred kilometers per second [74–76].

(iv) *Effective one-body:* As already described, EOB describes a binary as a test body orbiting in the space-

time of a ''deformed'' black hole, with the deformation controlled by factors such as the mass ratio of the binary. Damour and Gopakumar [77] first examined the issue of how to compute recoil within the EOB framework, analytically identifying the major contributions to the recoil that accumulates over a coalescence, including the importance of the final merger and recoil waves in providing an ''antikick'' contribution. By calibrating some parameters of the EOB framework with results from numerical relativity, EOB has had great success generating waveforms and recoil velocities that match well with those from numerical relativity [78,79].

With the exception of the superkick configuration, all of these techniques predict recoils that peak at roughly a few hundred kilometers per second (depending on mass ratio, spins, and spin-orbit orientation; see [80] for detailed discussion and statistical analysis). This is substantially lower than the peak predicted by Fitchett's original calculation; his overestimate can be ascribed to neglect of important curved spacetime radiation emission and propagation effects.

In addition to their potential astrophysical applications, recoil computations serve another important purpose: They are a common point of comparison for these four approaches to strong-field gravity. The recoil velocity from a merging binary is calculated by integrating the emitted radiation over some number of orbits. Any significant systematic error in the approach used will tend to magnify the error in the estimated recoil velocity. Thus, the evaluated recoils for a range of black hole spins and mass ratios serve as a good platform for comparing various approaches to strong-field binary models.

C. This paper

Our goal is to revisit and improve the estimate of black hole recoil via black hole perturbation theory that was originally developed in Ref. [66]. That analysis predicts upper and lower bounds which are rather widely separated. This is because the analysis of [66] could not accurately model wave emission from the final plunge and merger. Using the time-domain perturbation theory code developed and presented in Refs. [53,54], we can now compute the contribution of those waves. As we describe in more detail in Sec. V, doing so completely reverses the conclusions of Ref. [66] regarding how the kick behaves as a function of spin. In particular, including the plunge and merger is crucial to correctly computing the ''antikick,'' the out-of-phase contribution to the recoil that arises from the merger's final GWs. This contribution to a binary's total recoil was first identified and characterized by Schnittman *et al.* [81]. We find that the inability to include this contribution in Ref. [66] is largely responsible for the large error bars in that analysis.

We begin by reviewing in Sec. II how we construct the worldline which the smaller member of our binary follows as it spirals into the larger black hole. As briefly described above, we break this trajectory into a slowly evolving ''inspiral'' (Sec. II A) followed by a transitional regime (Sec. II B) that takes the binary into a final plunge and merger (Sec. II C). This review is left general, so that in principle one could describe these dynamics for generic orbital geometry. We specialize in our analysis here to the simplest circular and equatorial orbits (Sec. II D).

We next briefly review how we compute gravitational radiation from a body moving on this trajectory. As mentioned above, our approach is based on finding solutions to the Teukolsky equation [82] for Kerr black hole perturbations. We review this equation's general properties in Sec. III, and then discuss the principles behind solving it in the frequency domain (Sec. III A) and in the time domain (Sec. III B). Section IV summarizes how one computes the radiation's linear momentum and the recoil of a merged system.

Section V presents the results of our analysis. We begin in Sec. V A with general considerations on how our results scale with mass ratio. Because we work strictly within the context of linearized perturbation theory, all of our results can be easily scaled to different mass ratios, provided that the scaling does not change the system so much that the validity of perturbation theory breaks down. Reference [66] argued that a modified scaling would allow us to estimate with reasonable accuracy quantities related to the recoil even out of the perturbative regime. Although those arguments are valid during the adiabatic inspiral, they break down when the members of the binary merge.

In Sec. V B, we then discuss in some detail the gravitational waveform we find for binary coalescence in the large mass ratio limit. We examine the different multipolar contributions to the last several dozen cycles of inspiral, followed by the plunge and merger. These examples illustrate the manner in which the coalescence waves very naturally evolve into a ''ringdown'' form. As discussed in some detail in Sec. III B, this behavior arises by virtue of how the Teukolsky equation's source term goes to zero, so that its solutions transition to their homogeneous form, as the infalling body approaches the large black hole's event horizon. Mino and Brink [57] first appear to have exploited this behavior, which was also seen in recent work by Lousto, Nakano, Zlochower, and Campanelli [56]. This demonstrates the power of perturbative methods at modeling physically important aspects of the merger waves.

Section V C examines the recoil that arises from these waves, focusing on how it depends (for the circular, equatorial case that we study) on the spin of the larger black hole. This analysis demonstrates very clearly the impact of the antikick first reported by Schnittman *et al.* [81]. With the antikick taken into account, the smallest recoils come from the largest spins when the merger is in a prograde sense; the largest spins come from retrograde mergers with large spins. The waves which give the system its antikick

come from those produced by the final plunge and merger, demonstrating very clearly the substantial impact these waves have on the system. We conclude this section by briefly discussing the convergence of our recoil results as a function of black hole spin. Interestingly, we find that the number of modes we must include in order for our results to converge is a strong function of the black hole's spin—rapid spin, prograde cases need more modes than do slow spin cases, which in turn need more modes than rapid spin, retrograde cases. We conclude the paper by discussing in Sec. VI how these tools may be used to expand the reach of two-body modeling in general relativity, and our future plans.

Throughout our analysis we generally use units in which $G = c = 1$. We sometimes use $c = 3 \times 10^5$ km/sec in order to present kicks in "physical" units.

II. BUILDING THE INSPIRAL AND PLUNGE TRAJECTORY

Roughly speaking, our coalescence model has two ingredients. First, we compute the worldline that the small body follows as it spirals from large radius through plunge into the black hole. We then use that worldline to build the source for the Teukolsky equation and compute the GWs that are generated as the smaller body follows the worldline into the black hole. Though for simplicity we describe these ingredients as though they stand in isolation, they are in fact strongly coupled. We describe here how we compute the inspiral and plunge trajectory, deferring discussion of how we compute radiation from this trajectory to Sec. III. Throughout, we indicate how these steps are coupled to one another.

The trajectory which the small body follows can be broken into three pieces: An early time *inspiral*, in which the smaller member of the binary is approximated as evolving through a sequence of bound orbits of the larger black hole; a late-time *plunge*, in which the small body falls into the larger black hole; and an intermediate *transition* which smoothly connects these two regimes. We now briefly review how we model these different pieces.

In all of these regimes, we treat the zeroth order motion of the small body as a geodesic of the Kerr spacetime. These geodesics must be augmented by the conservative action of a self force if one's goal is to make a model that faithfully reproduces the phase of binary black hole GWs. For our present goal of estimating the GW recoil, we expect that the error due to neglecting this force is not important. Kerr black hole geodesics [83] are described by the following equations for the motion in Boyer-Lindquist coordinates r, θ, ϕ, and t:

$$\Sigma \frac{dr}{d\tau} = \pm\sqrt{R}, \tag{2.1}$$

$$\Sigma \frac{d\theta}{d\tau} = \pm\sqrt{V_\theta}, \tag{2.2}$$

$$\Sigma \frac{d\phi}{d\tau} = V_\phi, \tag{2.3}$$

$$\Sigma \frac{dt}{d\tau} = V_t. \tag{2.4}$$

The potentials appearing here are

$$R = [E(a^2 + r^2) - aL_z]^2 - \Delta[(L_z - aE)^2 + \mu^2 r^2 + Q], \tag{2.5}$$

$$V_\theta = Q - \cos^2\theta[a^2(\mu^2 - E^2) + \csc^2\theta L_z^2], \tag{2.6}$$

$$V_\phi = \csc^2\theta L_z - aE + \frac{a}{\Delta}[E(r^2 + a^2) - L_z a], \tag{2.7}$$

$$V_t = a(L_z - aE\sin^2\theta) + \frac{r^2 + a^2}{\Delta}[E(r^2 + a^2) - L_z a]. \tag{2.8}$$

The quantity M is the large black hole's mass, a is that hole's Kerr spin parameter, and μ is the mass of the smaller body which perturbs the black hole spacetime. The functions $\Sigma = r^2 + a^2\cos^2\theta$ and $\Delta = r^2 - 2Mr + a^2$. In the absence of radiation emission, the energy E, axial angular momentum L_z, and Carter constant Q are constants of the motion; up to initial conditions, choosing these three constants defines a geodesic.

Equations (2.1), (2.2), (2.3), and (2.4) are the starting point for building the smaller body's inspiral and plunge worldline. We now describe in some detail how we use them for this computation.

A. The inspiral

We approximate the inspiral as a slowly evolving sequence of bound Kerr geodesics (neglecting for now conservative aspects of the self interaction). Momentarily ignore the impact of radiation emission. In this limit, the orbits are determined by selecting E, L_z, and Q plus initial conditions, and are completely characterized by three orbital frequencies describing their periodic motions in the r, θ, and ϕ coordinates [84]. This periodic nature means that functions built from the orbital motion can be usefully represented by a discrete Fourier expansion.

To build our inspiral, we assume that radiation acts slowly enough that, to a good approximation, we can treat the small body's worldline as a Kerr geodesic at each moment. We then use the frequency-domain Teukolsky solver described in Sec. III to compute the rates at which E, L_z, and Q evolve due to GW backreaction. From these rates of change, we build the time-varying parameters $E(t)$, $L_z(t)$, and $Q(t)$ which describes the sequence of orbits the

small body passes through on its inspiral. More detailed discussion of this procedure is given in Refs. [55,85].

B. The last stable orbit and the transition to plunge

Our assumptions, and hence our procedure for computing the inspiral, break down as the small body approaches the *last stable orbit*, or LSO. This is worth describing in some detail. For bound orbits, the function $R(r)$ defined in Eq. (2.5) generally has four real roots. Denote these roots $r_1 > r_2 > r_3 > r_4$. The root r_4 is generally inside the event horizon,[3] and is not interesting for our discussion. The roots r_1, r_2, and r_3 on the other hand, are quite important. When these roots are distinct, the geodesic describes an eccentric orbit that oscillates between r_1 (apoapsis) and r_2 (periapsis). When $r_1 = r_2 > r_3$, the geodesic describes a circular orbit at $r = r_1$. (In this case, we also have $dR/dr = 0$ at $r = r_1$.) When $r_2 = r_3$, the orbit is *marginally stable*. (The triple root $r_1 = r_2 = r_3$ denotes a marginally stable circular orbit.) Once we reach this point, the small body will rapidly plunge into the black hole. This condition defines the LSO.

As inspiral proceeds, the roots r_2 and r_3 approach one another, indicating that GW backreaction is carrying the small body toward the LSO. We model the transition from slowly evolving geodesics through the LSO to plunge by expanding the equations of motion around their behavior at the LSO, as described in Ref. [58] (which generalizes Ref. [59]). More specifically, we take the constants in the transition to be given by

$$E(t) \simeq E_{\rm LSO} + (t - t_{\rm LSO})\dot{E}_{\rm LSO}, \tag{2.9}$$

and similarly for L_z and Q. Here, $E_{\rm LSO}$ and $\dot{E}_{\rm LSO}$ are the energy and its rate of change at the LSO (the latter calculated using our frequency-domain Teukolsky equation solver), and $t_{\rm LSO}$ is the time at which the LSO is reached. We integrate the geodesic equations using this form from a time $t_{\rm start} < t_{\rm LSO}$ until a time $t_{\rm end} > t_{\rm LSO}$. Reference [58] describes how we choose $t_{\rm start}$ and $t_{\rm end}$ as a function of parameters such as the black hole spin a and binary mass ratio. For our purposes, it is enough to note that, provided they are chosen within a well-defined range, our results are robust to that choice—varying $t_{\rm start}$ and $t_{\rm end}$ does not significantly change the recoil. A more careful investigation may clarify the optimal way to define these transition parameters.

C. The plunge

For $t > t_{\rm LSO}$, the geodesics described by $E(t)$, $L_z(t)$, and $Q(t)$ correspond to plunging geodesics, i.e., trajectories which fall into the large black hole. As described in Ref. [58], the transition matches onto a plunging trajectory most simply by just holding these parameters constant for $t \geq t_{\rm end}$. This is justified by the fact that radiation reaction does not have a strong impact in the final plunge [46,47,86]: careful analysis indicates that an orbit's energy and angular momentum remain nearly constant during the final plunge into the black hole.

As the small body approaches the black hole, its motion as viewed by distant observers appears to "freeze" onto the generators of the event horizon.[4] When this happens, the source term of the Teukolsky equation redshifts to zero [cf. Eq. (2.46) of Ref. [53]]. Since the homogeneous Teukolsky equation's solutions are the quasinormal modes of the binary's large black hole, this means that the final cycles of radiation from our coalescing system are very naturally given by the system's ringdown modes.

D. Specialization to circular equatorial orbits

Until now, we have kept the discussion of these inspiral and plunge trajectories general in order to emphasize that our approach can be applied to totally generic coalescences. For this first analysis, we now focus on the simplest interesting case, circular orbits confined to the equatorial plane of the larger black hole. In this limit, geodesic orbits are totally characterized by the orbit's radius; Ref. [83] gives an outstanding summary of their properties.

The energy, angular momentum, and Carter constant of circular equatorial orbits are given by

$$E = \frac{1 - 2M/r \pm aM^{1/2}/r^{3/2}}{\sqrt{1 - 3M/r \pm 2aM^{1/2}/r^{3/2}}}, \tag{2.10}$$

$$L_z = \pm \frac{\sqrt{rM}(1 \mp 2aM^{1/2}/r^{3/2} + a^2/r^2)}{\sqrt{1 - 3M/r \pm 2aM^{1/2}/r^{3/2}}}, \tag{2.11}$$

$$Q = 0. \tag{2.12}$$

Upper sign refers to prograde coalescences (orbital angular momentum parallel to black hole spin), lower sign to retrograde (antiparallel). These orbits are characterized by a single frequency associated with the azimuthal motion,

$$\Omega = \Omega_\phi = \pm \frac{M^{1/2}}{r^{3/2} \pm aM^{1/2}}. \tag{2.13}$$

The last stable orbit is located at

$$r_{\rm lso}/M = 3 + Z_2 \mp \sqrt{(3 - Z_1)(3 + Z_1 + 2Z_2)}, \tag{2.14}$$

$$Z_1 = 1 + (1 - a^2/M^2)^{1/3} \times [(1 + a/M)^{1/3} + (1 - a/M)^{1/3}], \tag{2.15}$$

[3] In fact, $r_4 = 0$ for equatorial orbits ($Q = 0$) and for orbits of Schwarzschild black holes ($a = 0$).

[4] This behavior led many researchers to call these solutions "frozen stars" in the early literature.

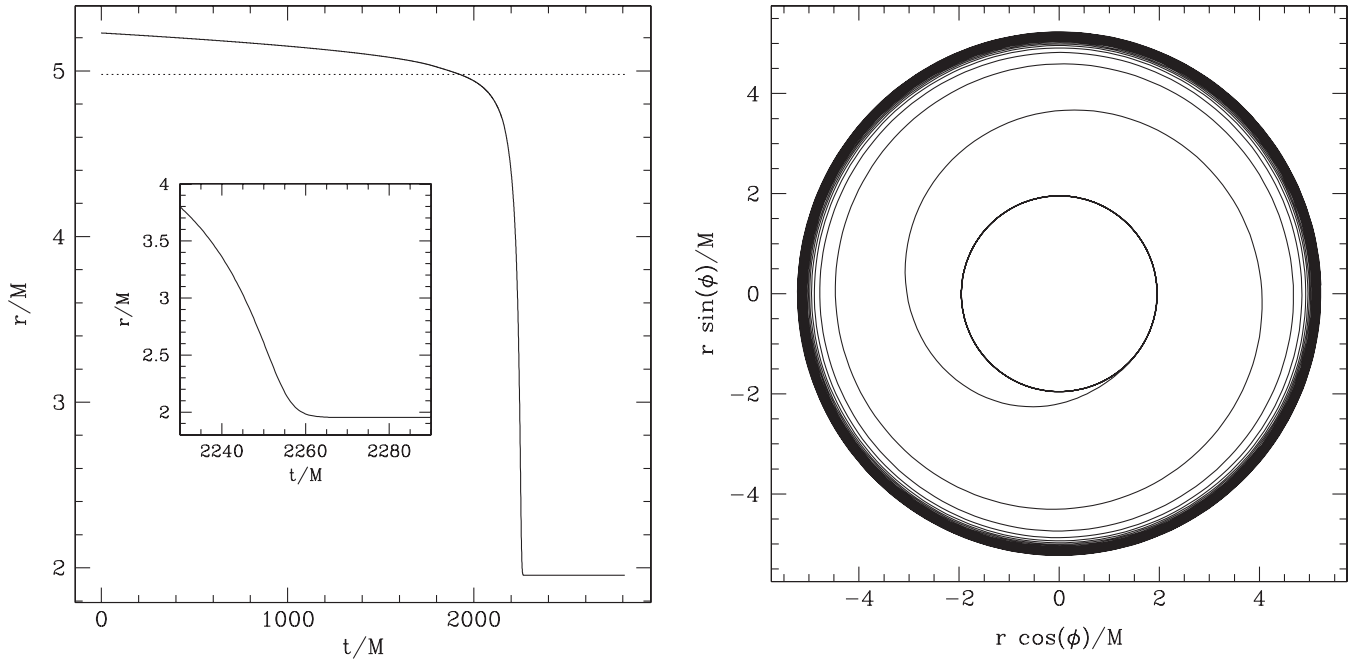

FIG. 1. Example quasicircular inspiral and plunge trajectory. For this calculation, the larger black hole's spin was set to $a = 0.3M$, and the binary's mass ratio is $\mu/M = 10^{-4}$. Left panel shows $r(t)$, the trajectory's radius as a function of time; right panel shows the same trajectory as viewed in the equatorial plane of the larger black hole. On the left, the dotted line at $r = 4.98M$ labels the radius of the prograde last stable orbit. Our trajectory, which starts at $r = 5.23M$, executes about 25 orbits before crossing this point. The inset there zooms in on the region $t \simeq 2260M$, showing the smaller body's trajectory as it approaches the event horizon at $r = 1.955M$. On the right, the heavy circle at $r = 1.955M$ is the hole's event horizon; notice how the particle quickly "locks" onto the horizon after the plunge which follows its slow inspiral.

$$Z_2 = \sqrt{Z_1^2 + 3a^2/M^2}. \tag{2.16}$$

Our procedure for building an inspiral and plunge trajectory reduces, in the equatorial circular limit, to the following algorithm:

(1) Choose a mass μ for the smaller body, and mass M and spin a for the larger black hole.[5] Pick an initial orbital radius r and an initial azimuth ϕ for the smaller body's trajectory.
(2) Evolve through a sequence of circular, equatorial orbits using $\dot{E}$ computed with the frequency-domain code (described in the following section). For these orbits, we do not need to compute $\dot{Q}$ since $Q = 0$ over the entire sequence. Also, in this case $\dot{L}_z$ is simply related to $\dot{E}$, so computing it does not provide additional information.
(3) As we approach the last stable orbit, switch to the transition trajectory following Ref. [58]. In particular, Ref. [58] describes how to choose the times at which we start and end the transition regime, which depends in detail on the system's mass ratio, the larger black hole's spin, and the orbit geometry. For circular, equatorial orbits, this prescription reduces to that given in Ref. [59].
(4) When we reach $t_{\rm end}$, hold the parameters E and L_z constant, and allow the small body to follow the plunging trajectory so defined into the larger black hole.

An example trajectory is shown in Fig. 1. For this figure, we examine a binary with a mass ratio $\mu/M = 10^{-4}$. The larger black hole has a spin $a = 0.3M$. We start our prograde trajectory at $r = 5.23M$, close to the LSO at $r = 4.98M$. The smaller body orbits roughly 25 times before crossing the LSO; shortly thereafter, it rapidly plunges into the black hole, locking onto the horizon as seen by distant observers. The inset in the left panel of Fig. 1 zooms in on its approach to the horizon, showing that our plunge trajectory smoothly asymptotes to the final "horizon locking" behavior.

III. COMPUTING RADIATION

We compute gravitational radiation from our model binaries using the Teukolsky equation, which describes the evolution of curvature perturbations to a Kerr black hole [82,87]. In Boyer-Lindquist coordinates, it is given by

[5] As is common with codes of this sort, we normalize most dimensionful quantities to M. As such, we really pick mass ratio μ/M; the impact of M can then be accounted for in post-processing after the numerics have been evaluated.

$$-\left[\frac{(r^2+a^2)^2}{\Delta}-a^2\sin^2\theta\right]\partial_{tt}\Psi-\frac{4Mar}{\Delta}\partial_{t\phi}\Psi - 2s\left[r-\frac{M(r^2-a^2)}{\Delta}+ia\cos\theta\right]\partial_t\Psi + \Delta^{-s}\partial_r(\Delta^{s+1}\partial_r\Psi)+\frac{1}{\sin\theta}\partial_\theta(\sin\theta\partial_\theta\Psi) + \left[\frac{1}{\sin^2\theta}-\frac{a^2}{\Delta}\right]\partial_{\phi\phi}\Psi+2s\left[\frac{a(r-M)}{\Delta}+\frac{i\cos\theta}{\sin^2\theta}\right]\partial_\phi\Psi - (s^2\cot^2\theta-s)\Psi=-4\pi(r^2+a^2\cos^2\theta)T, \quad (3.1)$$

where M is the mass of the black hole, a its angular momentum per unit mass, $\Delta=r^2-2Mr+a^2$, $r_\pm=M\pm\sqrt{M^2-a^2}$. The quantity s is the "spin weight" of the field under study. Choosing $s=0$ means the perturbing field is a scalar field; $s=\pm1$ describes a spin-1 (electromagnetic) perturbation, and $s=\pm2$ describes gravitational perturbations. For $s=+2$, the field Ψ is given by the Weyl curvature scalar ψ_0 (see [88] for precise definitions and discussion of this quantity); for $s=-2$, $\Psi=(r-ia\cos\theta)^4\psi_4$, where ψ_4 is another curvature scalar. We use $s=-2$ since ψ_4 is a natural choice to study outgoing radiation. Once ψ_4 is known, we then know the GWs that the binary produces, since

$$\psi_4\to\frac{1}{2}\left(\frac{\partial^2 h_+}{\partial t^2}-i\frac{\partial^2 h_\times}{\partial t^2}\right) \quad (3.2)$$

far from the black hole.

The T on the right hand side of Eq. (3.1) is a source term constructed from the stress-energy tensor describing a pointlike body moving in the Kerr spacetime. This stress-energy tensor is given by

$$T_{\alpha\beta}=\mu\int u_\alpha u_\beta\delta^{(4)}[\mathbf{x}-\mathbf{z}(\tau)]d\tau, \quad (3.3)$$

$$=\mu\frac{u_\alpha u_\beta}{\Sigma\dot{t}\sin\theta}\delta[r-r(t)]\delta[\theta-\theta(t)]\delta[\phi-\phi(t)]. \quad (3.4)$$

On the top line, $\mathbf{x}$ denotes an arbitrary spacetime event, $\mathbf{z}(\tau)$ describes the worldline that the point body follows, and τ is proper time along that worldline. On the second line, we have performed the integral and written the result in terms of the body's motion in the Boyer-Lindquist coordinates r, θ, and ϕ, parameterized by coordinate time t. On both lines, $u_\alpha=dz_\alpha/d\tau$ is the 4-velocity of the body as it moves along its worldline.

Note, in particular, the $\dot{t}\equiv dt/d\tau$ that appears in the denominator of Eq. (3.4). This is the timelike component of the smaller body's geodesic motion, described by Eq. (2.4). As the small body approaches the horizon, $\dot{t}\to\infty$—the passage of coordinate time (time as measured by distant observers) diverges per unit proper time as measured by that body. This is the mechanism by which the source term "redshifts away" as the small body falls into the large black hole, smoothly converting the Teukolsky equation into its homogeneous form.

The source T is constructed from this $T_{\alpha\beta}$ by projecting onto a tetrad that describes radiation, and then applying a particular integro-differential operator; see Refs. [52,53,82] for detailed discussion of its nature. For our purposes here, the key thing to note is that we must construct the worldline which the small body follows in order to compute the radiation associated with its motion. Different approximations are appropriate to different regimes of the coalescence, which is why we have developed two rather different codes for solving Eq. (3.1). We now briefly summarize the techniques behind these two codes, and how we use our solutions.

A. Radiation in the frequency domain

As was originally found by Teukolsky [82], Eq. (3.1) separates. For $s=-2$, we put

$$\psi_4=\frac{1}{(r-ia\cos\theta)^4}\int d\omega\sum_{lm}R_{lm\omega}(r)S_{lm}(\theta)e^{i(m\phi-\omega t)}. \quad (3.5)$$

The function $S_{lm}(\theta)$ is a spin-weighted spheroidal harmonic, and can be constructed by expanding on a basis of spin-weighted spherical harmonics [51]. The function $R_{lm\omega}(r)$ is found by solving a second-order ordinary differential equation. Its limiting behavior is

$$R_{lm\omega}(r\to\infty)\propto Z^\infty e^{i\omega r^*}, \quad (3.6)$$

corresponding to purely outgoing radiation far away, and

$$R_{lm\omega}(r\to r_+)\propto Z^H e^{-ikr^*}, \quad (3.7)$$

corresponding to purely ingoing radiation on the event horizon. The wave number $k=\omega-m\omega_+$, where $\omega_+=a/2Mr_+$ is the angular velocity of the hole's event horizon. In both of these equations, r^* is the so-called "tortoise coordinate,"

$$r^*=r+\frac{2Mr_+}{r_+-r_-}\ln\left(\frac{r-r_+}{2M}\right)-\frac{2Mr_-}{r_+-r_-}\ln\left(\frac{r-r_-}{2M}\right). \quad (3.8)$$

The ingoing and outgoing solution is thus characterized by the coefficients Z^∞ and Z^H. For details of how we compute these numbers, see Refs. [51,52].

This frequency-domain approach to solving Eq. (3.1) is most useful when the source T has a discrete frequency spectrum. The function ψ_4 can then be written as a sum over harmonics of the source's fundamental frequencies. This is the case for geodesic black hole orbits; see Ref. [52] for an extensive discussion.

For the circular, equatorial case, orbits and hence the source T are completely characterized by the frequency Ω_ϕ defined in Eq. (2.13). The frequency ω in Eq. (3.5) becomes $m\Omega_\phi$, and the coefficients Z^∞ and Z^H are then

determined by ω and the harmonic indices l and m. Once those coefficients are known, it is not difficult to compute the rates of change of E, L_z, and Q. The coefficients $Z^{\infty,H}$ are labeled by the indices l and m, and we have

$$\dot{E}^{\infty} = \sum_{lm} \frac{|Z^{\infty}_{lm}|^2}{4\pi\omega_m^2}, \tag{3.9}$$

$$\dot{L}_z^{\infty} = \sum_{lm} \frac{m|Z^{\infty}_{lm}|^2}{4\pi\omega_m^3}, \tag{3.10}$$

where $\omega_m = m\Omega_\phi$. Strictly speaking, the l sum appearing here is from $l = 2$ to infinity, and m is from $-l$ to l; in practice, the sums converge to double precision accuracy once l is of order a few to a few dozen, depending on how fast the smaller body orbits. See Refs. [51,52] for an extensive discussion of convergence issues, as well as for a discussion of how to compute the down-horizon contribution to the rates of change. Also, see Ref. [89] for a discussion of how to compute the rate of change of Q.

B. Radiation in the time domain

Because they work best when the source has a discrete frequency spectrum, we only use frequency-domain techniques to describe the inspiral, when the system is accurately described as slowly evolving through a sequence of orbits. When this description is not accurate (such as in the final plunge, or when inspiral is sufficiently rapid that the system does not spend many cycles near a given orbit), Eq. (3.5) is ill-suited to describing solutions of the Teukolsky equation. To handle this case, we solve Eq. (3.1) directly in the time domain.

In the code we have developed for this, we take advantage of the Kerr spacetime's axial symmetry to write the field Ψ as [53,54]

$$\Psi(t, r, \theta, \phi) = \sum_m e^{im\phi} r^3 \Phi_m(t, r, \theta). \tag{3.11}$$

Equation (3.1) is then solved as a $(2 + 1)$-dimensional partial differential equation for the modes Φ_m.

The major difficulty in numerically solving Eq. (3.1) is coming up with a good description of the source term. One challenge is to represent a pointlike source on a numerical grid [we use finite-difference techniques to solve Eq. (3.1)]. In Refs. [53,54], we have developed a discrete representation of a delta function which works very well on a finite-difference grid. This function is defined so that our representation of the delta function and of its first two derivatives preserves various integral identities. For cases in which a comparison can be made (e.g., for nonevolving generic geodesic orbits), we find that this representation allows us to compute GWs in the time domain with less than a 1% error compared to a frequency-domain code over a large span of orbital parameter space.

We use the transition and plunge trajectory described in the previous section to provide the worldline $\mathbf{z}(\tau)$ and 4-velocity u_α. As we have already highlighted, the Teukolsky Eq. (3.1) becomes homogeneous at late times thanks to the manner in which $\dot{t} \to \infty$ as the infalling body approaches the event horizon. When $T = 0$, the solutions of Eq. (3.1) are the larger black hole's quasinormal modes modes. This means that the late-time solution in our coalescence model is dominated by quasinormal modes of the larger black hole. By virtue of arising in a natural way from the behavior of our source term, these modes are properly phase connected to the preceding inspiral and plunge waves.

IV. COMPUTING RECOIL FROM RADIATION

Once we have computed ψ_4, it is not difficult to compute the rate at which linear momentum is carried by the waves. Letting $T^{\rm GW}_{\alpha\beta}$ denote the Isaacson [90] stress-energy tensor for GWs, we have

$$\begin{aligned}\frac{dP^i(t)}{dt} &= \lim_{r\to\infty} r^2 \int n^i T^{\rm GW}_{tt} d\Omega \\ &= \lim_{r\to\infty} \frac{r^2}{16\pi} \int n^i \left[\left(\frac{\partial h_+}{\partial t}\right)^2 + \left(\frac{\partial h_\times}{\partial t}\right)^2\right] d\Omega \\ &= \lim_{r\to\infty} \frac{r^2}{16\pi} \int n^i \left[\left(\frac{\partial h_+}{\partial t} - i\frac{\partial h_\times}{\partial t}\right)\right. \\ &\quad \left.\cdot \left(\frac{\partial h_+}{\partial t} + i\frac{\partial h_\times}{\partial t}\right)\right] d\Omega \\ &= \lim_{r\to\infty} \frac{r^2}{4\pi} \int n^i \left| \int_{-\infty}^{t} \psi_4 dt' \right|^2 d\Omega. \end{aligned} \tag{4.1}$$

The quantity n^i denotes the Cartesian direction vector in the large radius limit,

$$n^x \to \sin\theta\cos\phi, \tag{4.2}$$

$$n^y \to \sin\theta\sin\phi, \tag{4.3}$$

$$n^z \to \cos\theta. \tag{4.4}$$

This quantity must then be integrated over time to find the momentum carried by the GWs:

$$P^i(t) = \int_{-\infty}^{t} \frac{dP^i(t')}{dt} dt'. \tag{4.5}$$

Imposing global conservation of momentum, the recoil velocity of the system is then given by

$$v^i_{\rm rec}(t) = -P^i(t)/M. \tag{4.6}$$

Equation (4.6) will be our primary tool for computing black hole kicks in this analysis.

For the inspiral, which we model using frequency-domain methods, these formulas reduce to fairly simple results. In the $r \to \infty$ limit,

$$\psi_4 = \frac{1}{r}\sum_{lm} Z^{\infty}_{lm} S_{lm}(\theta) e^{im(\phi-\Omega_\phi t)}. \quad (4.7)$$

Inserting this expansion, the momentum flux formula (4.1) reduces to a sum over overlap integrals between different modes of the radiation field. This integral sharply constrains the mode numbers which contribute to this formulas sum. For Schwarzschild, the integral over θ can be expressed as a Clebsch-Gordan coefficient, and we find $l' \in [l-1, l, l+1]$; a similar but more complicated result describes the integral for Kerr. For any spin, we find $m' = m \pm 1$ for $P^x(t)$ and $P^y(t)$ [$P^z(t) = 0$ for the equatorial orbits we consider here]. Details of this calculation will be presented in a separate analysis [91]. For the final plunge and merger portions of the coalescence, we simply evaluate Eqs. (4.1), (4.5), and (4.6) using the ψ_4 computed with our time-domain code.

V. RESULTS: THE COALESCENCE WAVEFORM AND RECOIL

We now put the pieces of this formalism together to compute the waveforms from binary black hole coalescence and to calculate recoil. We begin by describing some issues with extrapolating from the truly perturbative mass ratios we study here (Sec. V A), and then describe in more detail how we assemble the full inspiral trajectory and its associated waveform (Sec. V B) before discussing our results for the recoil (Sec. V C). As already mentioned, we focus in this analysis on quasicircular equatorial configurations. We conclude (Sec. V D) by describing the convergence of our recoil results. We find that as we go to large spin, prograde mergers may require a large number of m modes [cf. the axial decomposition (3.11) we use] to give convergent results.

A. Mass ratio dependence considerations

By using the Teukolsky equation to model coalescence, we are by construction working to first order in mass ratio—the curvature scalar ψ_4 that we compute neglects all corrections of order $(\mu/M)^2$. Since the various fluxes we compute (energy, momentum, angular momentum) follow from the modulus squared of ψ_4, it likewise follows that these fluxes are all strictly proportional to $(\mu/M)^2$. The recoil velocity, as an integral of the momentum flux, should likewise scale essentially with $(\mu/M)^2$. We may expect small deviations from this scaling since the time scales of inspiral and of plunge and merger do not scale with mass ratio in quite the same way. However, we have found that a $(\mu/M)^2$ scaling describes the final recoil very accurately for all mass ratios more extreme than $\mu/M = 10^{-3}$; we have not examined mass ratios less extreme than this yet. Since the scaling with mass ratio is trivial, we will present detailed results for only one choice, $\mu/M = 10^{-4}$. In our summary figure for total recoil velocity as a function of spin (Fig. 5), we normalize our results by the scaling $(\mu/M)^2$.

In Ref. [66], it was argued that one can improve the ability of perturbation theory to extrapolate out of the perturbative regime by replacing the $(\mu/M)^2$ which describes the momentum flux and the recoil velocity with

$$f(\mu/M) = \left(\frac{\mu}{M}\right)^2 \sqrt{1 - \frac{4\mu}{M}}. \quad (5.1)$$

In this argument, it is claimed that in extrapolating out of the perturbative regime it is useful to interpret the small body's mass μ as the system's reduced mass, and the large black hole's mass M as the system's total mass. A similar interpretation of these masses has been shown to give excellent results interpreting the head-on collisions of black holes [92]. The function $f(\mu/M)$ has a maximum $f_{\max} = 0.01789$ at $\mu/M = 0.2$ (corresponding, after remapping the meaning of these mass parameters, to $m_{\text{small}}/m_{\text{large}} = 0.382$).

As we will discuss in more detail later in this section, using this scaling does not work quite as well as we might have hoped. The key issue is that in our perturbative framework, we assume there exists a stationary background spacetime which we can expand around, and that this background does not evolve during the coalescence. This means, for example, that a binary which contains a large Schwarzschild black hole at early times will evolve to a single Schwarzschild black hole at late times; we fail to account for the evolution of this black hole's spin during the merger. This is a minor error when the mass ratio is small, but is significant for large mass ratio. In particular, for mass ratios $\mu/M \sim 0.1$ or larger, the spin of the final black hole will change substantially in the merger. By not evolving the spin properly, we do not get the late-time spectrum of merger/ringdown waves correct, with important consequences for the system's final kick.

B. Example waveform

Figures 2–4 present coalescence waveforms for a binary with $\mu/M = 10^{-4}$, and in which the larger black hole has spin $a/M = 0.6, 0$, and -0.6 respectively. We focus on the late waves, including the final plunge and ringdown. The data for these figures were generated using the time-domain code discussed in Sec. III B. In the largest panel, we show the wave including all contributions with $|m| \leq 6$; the three smaller panels show individual contributions from the $m = 1$, 2, and 3 modes.

In all three examples we show, the general character of the waveforms is essentially the same: a slowly evolving chirping sinusoid that terminates in an exponentially damped ringdown. Two aspects of the waveforms clearly differ as we move from $a = 0.6M$ to $a = -0.6M$. First, notice that the waveform for $a = 0.6M$ is clearly of rather higher frequency than for $a = 0$, which in turn is higher

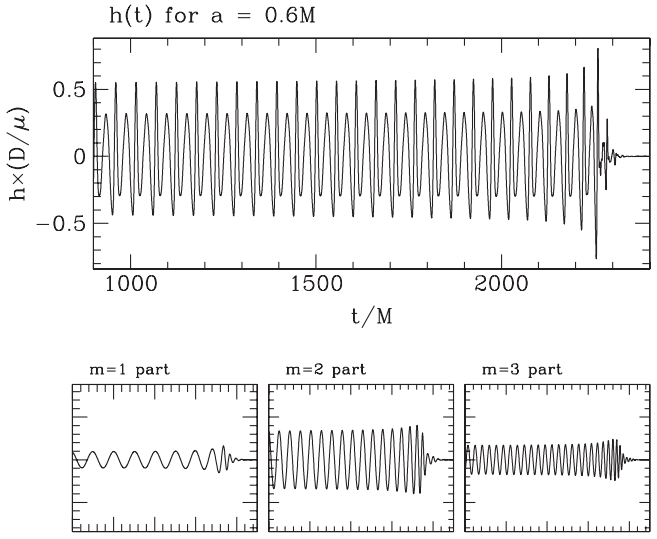

FIG. 2. Coalescence waveform computed with perturbation theory for a binary with mass ratio $\mu/M = 10^{-4}$, and in which the larger black hole has spin $a = 0.6M$. We show the $+$ polarization of the waveform as viewed in the binary's equatorial plane; the $\times$ waveform is zero from this viewing angle. The wave is normalized by D, the distance from source to observer, and the origin of the time axis is arbitrary. The waveform shown in the top panel includes contributions from all modes with $|m| \leq 6$; the individual contributions for $m = 1$, $m = 2$, and $m = 3$ are shown below. Notice how the smoothly chirping inspiral waves blend naturally into the rapidly damped ringdown which terminates this waveform.

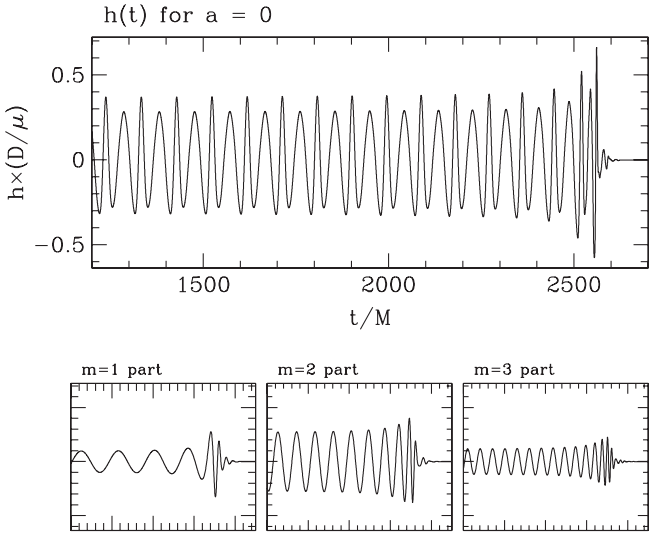

FIG. 3. Same as Fig. 2, but the large black hole has spin $a = 0$ in this case. The frequencies which describe this wave are generically lower than those shown in Fig. 2 since the transition from inspiral to plunge happens at larger radius thanks to smaller spin parameter in this binary. In addition, the final ringdown waves damp out more rapidly than in the $a = 0.6M$ case.

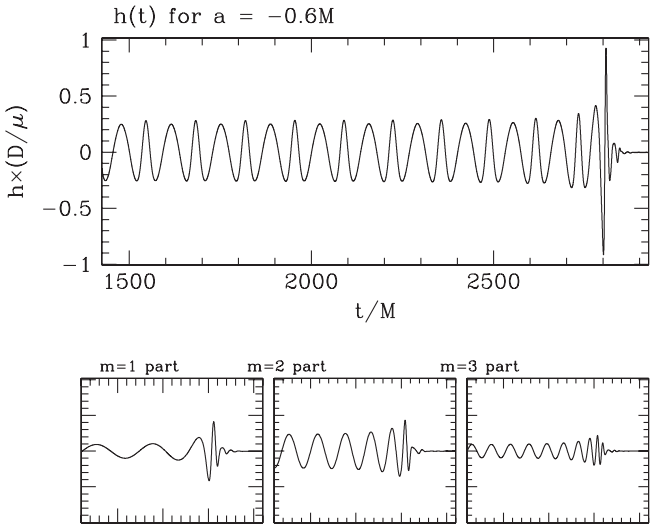

FIG. 4. Same as Figs. 2 and 3, but now for black hole spin $a = -0.6M$ (i.e., same black hole as in Fig. 2, but now for a retrograde orbit geometry). The frequencies characterizing this wave are again lower than for the two previous examples, and the ringdown waves damp even more rapidly.

than for $a = -0.6M$. This is not surprising, and is a simple consequence of the orbit's geometry: the LSO, which approximately delineates the transition from inspiral to final plunge, is at $r_{\rm LSO} = 3.83M$ for $a = 0.6M$, $r_{\rm LSO} = 6M$ for $a = 0$, and $r_{\rm LSO} = 7.85M$ for $a = -0.6M$. As the LSO moves to larger radius, the orbital frequency associated with it sweeps lower.

Second, the final ringdown waves damp more quickly as we move from the prograde to the retrograde configuration. This is also not surprising, and follows naturally from the damping behavior of a Kerr black hole's quasinormal modes: modes which are ''parallel'' to a hole's spin (i.e., have $m > 0$ for $a > 0$, and vice versa) are much more long lived than ''antiparallel'' modes. See, for example, Fig. 45 of Ref. [88] (noting that Chandra's sign convention on the Fourier transform means that $m_{\rm Chandra} = -m_{\rm us}$).

C. Recoil versus spin

Figure 5 summarizes how the kick imparted to a binary behaves as a function of spin for mass ratio $\mu/M = 10^{-4}$. In this plot, we show the magnitude of the recoil that has accumulated up to some time t. Since the origin of the time axis is not particularly interesting, we have shifted the various tracks so that we can easily compare how the recoil varies as a function of spin.

The clearest feature apparent here is that, especially for prograde coalescences ($a > 0$), the recoil grows to some large positive value, but then is strongly suppressed by an antikick to something significantly smaller. The suppression is a very strong function of the large black hole's spin: For the five cases which show antikick behavior in Fig. 5, the peak kick $v^{\rm peak}$ and the late-time kick $v^{\rm late}$ are given by

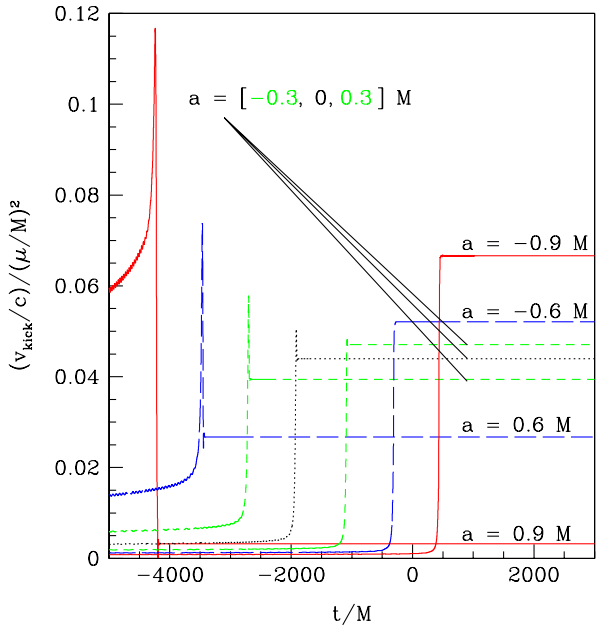

FIG. 5 (color online). Summary of recoil versus time for large black hole spins $a/M \in [-0.9, -0.6, -0.3, 0, 0.3, 0.6, 0.9]$. For each track, the time origin is arbitrary, so we have shifted the data in order to cleanly display all seven recoil trends shown here. The key feature we find is the manner in which (especially for large spin, prograde coalescences) the kick builds to a large positive value, followed by an antikick that brings the total accumulated recoil down to much smaller values. The antikick is especially strong when the spin is large and the coalescence is prograde, and is essentially nonexistent for large spin retrograde coalescence.

$$a = 0.9M\text{: } v^{\rm peak}/c = 0.17(\mu/M)^2$$
$$v^{\rm late}/c = 0.0032(\mu/M)^2; \quad (5.2)$$

$$a = 0.6M\text{: } v^{\rm peak}/c = 0.074(\mu/M)^2$$
$$v^{\rm late}/c = 0.027(\mu/M)^2; \quad (5.3)$$

$$a = 0.3M\text{: } v^{\rm peak}/c = 0.058(\mu/M)^2$$
$$v^{\rm late}/c = 0.039(\mu/M)^2; \quad (5.4)$$

$$a = 0\text{: } v^{\rm peak}/c = 0.051(\mu/M)^2$$
$$v^{\rm late}/c = 0.044(\mu/M)^2; \quad (5.5)$$

$$a = -0.3M\text{: } v^{\rm peak}/c = 0.048(\mu/M)^2$$
$$v^{\rm late}/c = 0.047(\mu/M)^2. \quad (5.6)$$

In other words, we find that the antikick suppresses the maximum recoil by a factor of 53 for $a = 0.9M$, 2.7 for $a = 0.6M$, 1.5 for $a = 0.3M$, 1.2 for $a = 0$, and 1.02 for $a = -0.3M$. The late-time kick shown in Fig. 5 is nicely fit by the formula

$$v_{\rm rec}(a)/c \simeq [0.0440 - 0.0099(a/M) - 0.0114(a/M)^2 - 0.0312(a/M)^3](\mu/M)^2. \quad (5.7)$$

Over most of the relevant parameter space, this comes in right between the "upper" and "lower" estimates of Ref. [66] [compare to Eqs. (1) and (2) of Ref. [93]].

The antikick behavior we see agrees at least qualitatively with the trends seen in Schnittman *et al.* [81]. It is hard to calibrate the quantitative agreement between these analyses, since (as discussed above in Sec. V A) extrapolating from the perturbative regime into that of the mass ratios considered in Ref. [81] is not as simple as the arguments in Ref. [66] would suggest. Consider the Schwarzschild coalescence results. If we use the $(\mu/M)^2 \to f(\mu/M)$ rule suggested in Ref. [66], we find

$$v^{\rm late}(a = 0) = 0.044 f(\mu/M)c \leq 235 \text{ km/ sec}. \quad (5.8)$$

On the second line, we have used $f_{\rm max} = 0.01789$ in order to estimate how large the kick can be in this case.

Taken at face value, this suggests that the recoil of Schwarzschild black holes has a maximum of 235 km/ sec, 34% higher than the maximum value of 175 km/ sec found in careful numerical relativity calculations [94]. However, in those numerical relativity calculations, the final black hole is not Schwarzschild, but has a spin $a \simeq 0.67M$. Figure 5 tells us we should expect a larger antikick when the final black hole is rapidly spinning. Applying the same extrapolation to our recoil data for $a = 0.6M$ (the nearest value to $a = 0.67M$ in our dataset) leads to

$$v^{\rm late}(a = 0.6M) = 0.027 f(\mu/M)c \leq 144 \text{ km/ sec}. \quad (5.9)$$

This is about 18% lower than the numerical relativity prediction. The lesson we take from this is that naive extrapolation from the small mass ratio regime does not give a good estimate of the final kick in the comparable mass case. Because the background spacetime is fixed, we do not accurately describe the system's final state and hence the last waves that it emits during the coalescence.

D. Convergence

As discussed in Sec. III B, our time-domain perturbation theory code expands the field Ψ in axial modes; cf. Eq. (3.11). The angular integral in Eq. (4.1) takes the form

$$\frac{dP_x}{dt} \propto \sum_{m,m'} \int_0^{2\pi} d\phi \cos\phi e^{i(m-m')\phi} \Phi_m \Phi^*_{m'}$$
$$\propto \sum_{m,m'} (\delta_{(m+1),m'} + \delta_{(m-1),m'}) \Phi_m \Phi^*_{m'}, \quad (5.10)$$

TABLE I. Convergence of recoil with azimuthal mode for $a = -0.6M$. First column is $m_{\rm max}$, the largest value of m we include. Second column is the value of $\dot{\mathcal{P}}$, the peak magnitude of the momentum flux normalized by $(\mu/M)^2$. The third column gives the percentage change in $\dot{\mathcal{P}}$ we find as we increase $m_{\rm max}$ from the previous value.

$m_{\rm max}$	$\dot{\mathcal{P}}$	% change
2	2.855×10^{-3}	-
3	4.030×10^{-3}	29.2%
4	4.557×10^{-3}	11.6%
5	4.807×10^{-3}	5.2%
6	4.930×10^{-3}	2.5%

$$\frac{dP_y}{dt} \propto \sum_{m,m'} \int_0^{2\pi} d\phi \sin\phi e^{i(m-m')\phi} \Phi_m \Phi^*_{m'} \propto \sum_{m,m'} (\delta_{(m+1),m'} - \delta_{(m-1),m'}) \Phi_m \Phi^*_{m'}. \quad (5.11)$$

Contributions from terms with $m = m'$ vanish; the recoil arises from beating between adjacent m modes.

The question we now address is how many m modes must be included in order to accurately compute the recoil. We have found that this is a strong function of black hole spin: When the black hole has large positive spin, many more modes are needed for convergence than for small or retrograde coalescence.

Tables I, II, and III summarize convergence data for three of the cases presented in Fig. 5. We show, as a function of $m_{\rm max}$ [the value of m and m' at which the sums in Eqs. (5.10) and (5.11) are terminated] the peak magnitude of the momentum flux normalized by $(\mu/M)^2$,

TABLE II. Convergence of momentum flux with m for $a = 0$. All details are as in Table I.

$m_{\rm max}$	$\dot{\mathcal{P}}$	% change
2	1.712×10^{-3}	-
3	4.188×10^{-3}	58.9%
4	5.508×10^{-3}	24.0%
5	6.182×10^{-3}	10.9%
6	6.532×10^{-3}	5.4%

TABLE III. Convergence of momentum flux with m for $a = 0.6M$. All details are as in Table I.

$m_{\rm max}$	$\dot{\mathcal{P}}$	% change
2	1.373×10^{-3}	-
3	7.488×10^{-3}	81.7%
4	1.105×10^{-2}	32.2%
5	1.302×10^{-2}	15.1%
6	1.412×10^{-2}	7.8%

$$\dot{\mathcal{P}} \equiv \left[\frac{\sqrt{(dP_x/dt)^2 + (dP_y/dt)^2}}{(\mu/M)^2}\right]_{\rm max}. \quad (5.12)$$

The "max" subscript means that we select the maximum of this quantity over the timespan for which we compute the momentum flux. This quantity is given in units of M^{-1}. We also show the percentage change in $\dot{\mathcal{P}}$ as we increase $m_{\rm max}$ by one.

Tables I, II, and III indicate that, once several modes have been computed, the fractional error in the momentum flux decreases by roughly a factor of 2 with each unit increase in m. However, the magnitude of the relative error is a rather strong function of black hole spin. For $a = -0.6M$, we find that going from $m_{\rm max} = 5$ to $m_{\rm max} = 6$ changes the momentum flux by only 2.5%. Including additional modes presumably will only produce percent-level changes. For $a = 0.6M$ by contrast, the flux changes by nearly 8% as $m_{\rm max}$ is increased from 5 to 6. Many modes are clearly needed to accurately compute the waves (and the recoil from these waves) as the large black hole's spin approaches the Kerr maximum.

VI. CONCLUSIONS AND FUTURE WORK

Now that numerical relativity has effectively solved the two-body problem in general relativity, a major task for researchers has become to explore the parameter space of binary coalescence. This will insure that wave models constructed as templates for GW data analysis fully encompass the range of behaviors that are likely in real binary mergers, and allow us to more fully understand the phenomenology of binary black hole merger astrophysics. In this analysis, we have demonstrated that perturbation theoretical techniques based on the Teukolsky equation are an excellent tool for extending the reach of our computations, allowing us to model large mass ratios that are challenging for 3 + 1 numerical simulations, but may be of astrophysical significance. Our analysis joins previous work by Damour and colleagues [46,47], Mino and Brink [57], and by Lousto and colleagues [56] which likewise used perturbation theory to model large mass ratio binaries. By using the Teukolsky equation, we can explore how the larger black hole's spin impacts the analysis, exemplified by our demonstration of how the previously identified antikick [81] strongly depends on this spin.

Two directions for future analysis strike us as particularly noteworthy. First, the major motivation for this work is that perturbation theory makes exploring parameter space computationally fast and simple. As such, it would be worthwhile to continue this exploration, examining how the waveform varies as a function of spin-orbit alignment, and exploring (for example) how the antikick evolves as one varies the inclination smoothly from the prograde to the retrograde geometry. Preliminary calculations of this

behavior indicate that the antikick rapidly evolves with spin-orbit alignment, consistent with the results of Mino and Brink [57] which demonstrate a strong dependence on the final kick with the plunge geometry.

Second, as Damour and Nagar have emphasized [47], particularly useful application comes by including input from the effective one-body formalism in our description of the small body's motion; input from perturbation theory can likewise be used to calibrate certain parameters in the EOB framework. Now that the spin-augmented Hamiltonian for binary systems is understood [95,96], we expect that work to extend EOB to more broadly include the impact of spin will become very active. We hope that the tools we have presented here will be useful for further refining what has already proved to be a valuable tool for modeling coalescing binaries.

ACKNOWLEDGMENTS

We gratefully acknowledge helpful correspondence and discussion with T. Damour and A. Nagar regarding the literature on black hole perturbation theory and the effective one-body approach; we also thank T. Damour for useful feedback on a draft of this paper. We likewise thank C. Lousto and H. Nakano for helpful comments on an earlier version. A very early draft of this manuscript was presented as a chapter in the Ph.D. thesis of P. A. S. [97]. This work was supported at MIT by NASA Grant No. NNG05G105G and NSF Grant No. PHY-0449884. G. K. acknowledges research support from NSF Grant Nos. PHY-0831631 and PHY-0902026, and hardware donations from Sony and IBM. S. A. H. gratefully acknowledges the support of the A. J. Burgasser Chair in Astrophysics in completing this analysis.

[1] F. Pretorius, Phys. Rev. Lett. **95**, 121101 (2005).
[2] M. Campanelli, C. O. Lousto, P. Marronetti, and Y. Zlochower, Phys. Rev. Lett. **96**, 111101 (2006).
[3] J. G. Baker, J. Centrella, D.-I. Choi, M. Koppitz, and J. van Meter, Phys. Rev. Lett. **96**, 111102 (2006).
[4] F. Herrmann, I. Hinder, D. Shoemaker, and P. Laguna, Classical Quantum Gravity **24**, S33 (2007).
[5] E. Berti, V. Cardoso, J. A. Gonzalez, U. Sperhake, M. Hannam, S. Husa, and B. Brügmann, Phys. Rev. D **76**, 064034 (2007).
[6] M. Campanelli, C. O. Lousto, and Y. Zlochower, Phys. Rev. D **74**, 041501 (2006).
[7] M. Campanelli, C. O. Lousto, and Y. Zlochower, Phys. Rev. D **74**, 084023 (2006).
[8] M. Campanelli, C. O. Lousto, Y. Zlochower, B. Krishnan, and D. Merritt, Phys. Rev. D **75**, 064030 (2007).
[9] M. Campanelli, C. O. Lousto, H. Nakano, and Y. Zlochower, Phys. Rev. D **79**, 084010 (2009).
[10] I. Hinder, B. Vaishnav, F. Herrmann, D. Shoemarker, and P. Laguna, Phys. Rev. D **77**, 081502 (2008).
[11] I. Hinder, F. Herrmann, P. Laguna, and D. Shoemaker, arXiv:0806.1037.
[12] L. Blanchet, Living Rev. Relativity **9**, 4 (2006).
[13] A. Buonanno and T. Damour, Phys. Rev. D **59**, 084006 (1999).
[14] A. Buonanno and T. Damour, Phys. Rev. D **62**, 064015 (2000).
[15] T. Damour, P. Jaronowski, and G. Schaefer, Phys. Rev. D **62**, 084011 (2000).
[16] T. Damour, Phys. Rev. D **64**, 124013 (2001).
[17] A. Buonanno, Y. Pan, J. G. Baker, J. Centrella, B. J. Kelly, S. T. McWilliams, and J. R. van Meter, Phys. Rev. D **76**, 104049 (2007).
[18] T. Damour, A. Nagar, M. Hannam, S. Husa, and B. Brügmann, Phys. Rev. D **78**, 044039 (2008).
[19] T. Damour and A. Nagar, Phys. Rev. D **79**, 081503 (2009).
[20] A. Buonanno, Y. Pan, H. P. Pfeiffer, M. A. Scheel, L. T. Buchman, and L. E. Kidder, Phys. Rev. D **79**, 124028 (2009).
[21] J. Kormendy and K. Gebhardt, in *20th Texas Symposium on Relativistic Astrophysics*, AIP Conf. Series No. 586 (AIP, New York, 2001), p. 363.
[22] L. Ferrarese, in *Current High-Energy Emission Around Black Holes*, edited by C.-H. Lee and H.-Y. Chang (World Scientific, Singapore, 2002), p. 3.
[23] M. C. Begelamn, R. D. Blandford, and M. J. Rees, Nature (London) **287**, 307 (1980).
[24] http://lisa.nasa.gov.
[25] http://sci.esa.int/home/lisa/.
[26] A. Sesana, M. Volonteri, and F. Haardt, Mon. Not. R. Astron. Soc. **377**, 1711 (2007).
[27] S. Komossa, V. Burwitz, G. Hasinger, P. Predehl, J. S. Kaastra, and Y. Ikebe, Astrophys. J. Lett. **582**, L15 (2003).
[28] H. L. Maness, G. B. Taylor, R. T. Zavala, A. B. Peck, and L. K. Pollack, Astrophys. J. **602**, 123 (2004).
[29] C. Rodriguez, G. B. Taylor, R. T. Zavala, A. B. Peck, L. K. Pollack, and R. W. Romani, Astrophys. J. **646**, 49 (2006).
[30] H. Zhou, T. Wang, X. Zhang, X. Dong, and C. Li, Astrophys. J. Lett. **604**, L33 (2004).
[31] B. F. Gerke, J. A. Newman, J. Lotz, R. Yan, P. Barmby *et al.*, Astrophys. J. Lett. **660**, L23 (2007).
[32] M. J. Valtonen, H. J. Lehto, K. Nilsson, J. Heidt, L. O. Takalo *et al.*, Nature (London) **452**, 851 (2008).
[33] http://www.ligo.caltech.edu; http://www.ligo.org.
[34] http://www.virgo.infn.it/.
[35] http://www.geo600.org/.
[36] http://gw.icrr.u-tokyo.ac.jp/lcgt/.
[37] http://www.aigo.org.au/.
[38] http://www.et-gw.eu.
[39] L. Yungelson and S. F. Portegies Zwart, in *Second Workshop on Gravitational Wave Data Analysis*, edited by M. Davier and P. Hello (Editions Frontiéres, Paris, 1997), p. 77.
[40] K. A. Postnov and M. E. Prokhorov, in *Proceedings of the*

34th Recontres de Moriond, Gravitational Waves and Experimental Gravity (1999).
[41] S. F. Portegies Zwart and S. L. W. McMillan, Astrophys. J. Lett. **528**, L17 (2000).
[42] R. M. O'Leary, R. O'Shaugnessy, and F. A. Rasio, Phys. Rev. D **76**, 061504 (2007).
[43] A. D. Mackey, M. I. Wilkinson, M. B. Davies, and G. F. Gilmore, Mon. Not. R. Astron. Soc. **386**, 65 (2008).
[44] J. R. Gair, L. Barack, T. Creighton, C. Cutler, S. L. Larson, E. S. Phinney, and M. Vallisneri, Classical Quantum Gravity **21**, S1595 (2004).
[45] S. A. Hughes, AIP Conf. Proc. **873**, 233 (2006).
[46] A. Nagar, T. Damour, and A. Tartaglia, Classical Quantum Gravity **24**, S109 (2007).
[47] T. Damour and A. Nagar, Phys. Rev. D **76**, 064028 (2007).
[48] T. Regge and J. A. Wheeler, Phys. Rev. **108**, 1063 (1957).
[49] F. Zerilli, Phys. Rev. Lett. **24**, 737 (1970).
[50] S. A. Teukolsky, Astrophys. J. **185**, 635 (1973).
[51] S. A. Hughes, Phys. Rev. D **61**, 084004 (2000).
[52] S. Drasco and S. A. Hughes, Phys. Rev. D **73**, 024027 (2006).
[53] P. A. Sundararajan, G. Khanna, and S. A. Hughes, Phys. Rev. D **76**, 104005 (2007).
[54] P. A. Sundararajan, G. Khanna, S. A. Hughes, and S. Drasco, Phys. Rev. D **78**, 024022 (2008).
[55] S. A. Hughes, S. Drasco, E. E. Flanagan, and J. Franklin, Phys. Rev. Lett. **94**, 221101 (2005).
[56] C. O. Lousto, H. Nakano, Y. Zlochower, and M. Campanelli, Phys. Rev. Lett. (to be published); arXiv:1001.2316.
[57] Y. Mino and J. Brink, Phys. Rev. D **78**, 124015 (2008).
[58] P. A. Sundararajan, Phys. Rev. D **77**, 124050 (2008).
[59] A. Ori and K. S. Thorne, Phys. Rev. D **62**, 124022 (2000).
[60] W. B. Bonnor and M. A. Rotenberg, Proc. R. Soc. A **265**, 109 (1961).
[61] A. Peres, Phys. Rev. **128**, 2471 (1962).
[62] J. D. Bekenstein, Astrophys. J. **183**, 657 (1973).
[63] M. J. Fitchett, Mon. Not. R. Astron. Soc. **203**, 1049 (1983).
[64] I. H. Redmount and M. J. Rees, Comments Astrophys. **14**, 165 (1989).
[65] M. J. Fitchett and S. Detweiler, Mon. Not. R. Astron. Soc. **211**, 933 (1984).
[66] M. Favata, S. A. Hughes, and D. E. Holz, Astrophys. J. **607**, L5 (2004).
[67] R. H. Price and J. Pullin, Phys. Rev. Lett. **72**, 3297 (1994).
[68] C. F. Sopuerta, N. Yunes, and P. Laguna, Phys. Rev. D **74**, 124010 (2006).
[69] L. Blanchet, M. S. S. Qusailah, and C. M. Will, Astrophys. J. **635**, 508 (2005).
[70] A. Le Tiec, L. Blanchet, and C. Will, Classical Quantum Gravity **27**, 012001 (2010).
[71] M. Campanelli, C. O. Lousto, Y. Zlochower, and D. Merritt, Astrophys. J. **659**, L5 (2007).
[72] J. A. González, M. Hannam, U. Sperhake, B. Brügmann, and S. Husa, Phys. Rev. Lett. **98**, 231101 (2007).
[73] M. Campanelli, C. O. Lousto, Y. Zlochower, and D. Merritt, Phys. Rev. Lett. **98**, 231102 (2007).
[74] J. G. Baker, W. D. Boggs, J. Centrella, B. J. Kelly, S. T. McWilliams, M. C. Miller, and J. R. van Meter, Astrophys. J. **668**, 1140 (2007).
[75] J. G. Baker, W. D. Boggs, J. Centrella, B. J. Kelly, S. T. McWilliams, M. C. Miller, and J. R. van Meter, Astrophys. J. **682**, L29 (2008).
[76] C. O. Lousto and Y. Zlochower, Phys. Rev. D **79**, 064018 (2009).
[77] T. Damour and A. Gopakumar, Phys. Rev. D **73**, 124006 (2006).
[78] J. D. Schnittman and A. Buonanno, Astrophys. J. **662**, L63 (2007).
[79] T. Damour, Int. J. Mod. Phys. A **23**, 1130 (2008).
[80] C. O. Lousto, H. Nakano, Y. Zlochower, and M. Campanelli, Phys. Rev. D (to be published); arXiv:0910.3197.
[81] J. D. Schnittman, A. Buonanno, J. R. van Meter, J. G. Baker, W. D. Boggs, J. Centrella, B. J. Kelley, and S. T. McWilliams, Phys. Rev. D **77**, 044031 (2008).
[82] S. A. Teukolsky, Astrophys. J. **185**, 635 (1973).
[83] J. M. Bardeen, W. H. Press, and S. A. Teukolsky, Astrophys. J. **178**, 347 (1972).
[84] W. Schmidt, Classical Quantum Gravity **19**, 2743 (2002).
[85] S. A. Hughes, Phys. Rev. D **64**, 064004 (2001).
[86] A. Buonanno and T. Damour, in *The Ninth Marcel Grossmann Meeting: Proceedings of the MGIXMM Meeting*, edited by V. G. Gurzadyan, R. T. Jantzen, and R. Ruffini (World Scientific Publishing, Singapore, 2002), p. 1637.
[87] S. A. Teukolsky, Phys. Rev. Lett. **29**, 1114 (1972).
[88] S. Chandrasekhar, *The Mathematical Theory of Black Holes* (Oxford University Press, Oxford, 1983).
[89] N. Sago, T. Tanaka, W. Hikida, K. Ganz, and H. Nakano, Prog. Theor. Phys. **115**, 873 (2006).
[90] R. A. Isaacson, Phys. Rev. **166**, 1272 (1968).
[91] M. Favata, D. E. Holz, and S. A. Hughes (unpublished).
[92] L. Smarr, in *Sources of Gravitational Radiation*, edited by L. Smarr (Cambridge University Press, Cambridge, England, 1978), p. 267.
[93] D. Merritt, M. Milosavljevic, M. Favata, S. A. Hughes, and D. E. Holz, Astrophys. J. Lett. **607**, L9 (2004).
[94] J. A. Gonzalez, U. Sperhake, B. Brügman, M. Hannam, and S. Husa, Phys. Rev. Lett. **98**, 091101 (2007).
[95] T. Damour, P. Jaronowski, and G. Schäfer, Phys. Rev. D **77**, 064032 (2008).
[96] E. Barausse, E. Racine, and A. Buonanno, Phys. Rev. D **80**, 104025 (2009).
[97] P. A. Sundararajan, Ph.D. thesis, Massachusetts Institute of Technology, 2009.